PCCP

PAPER

Cite this: *Phys. Chem. Chem. Phys.*, 2019, **21**, 22238

The ionization energy of the vinyl radical: a Mexican standoff with a happy ending

Xiangkun Wu,[ab] Xiaoguo Zhou,[*b] Patrick Hemberger[a] and Andras Bodi[*a]

Received 13th August 2019,
Accepted 18th September 2019

DOI: 10.1039/c9cp04493k

rsc.li/pccp

The Active Thermochemical Tables (ATcT) yield 8.477 ± 0.007 eV as the ionization energy of the vinyl radical, which agrees with wave function theory results. The photoionization spectrum yielded 8.59 ± 0.03 eV, while the photoelectron spectrum yielded 8.25 ± 0.05 eV for the adiabatic ionization energy. In order to reconcile these contradictory measurements, we produced the vinyl radical by flash pyrolysis of divinyl sulfone, and recorded its photoionization (PI) and threshold photoelectron (TPE) spectrum in the 8.10–10.45 eV photon energy range at the Swiss Light Source for the first time using double imaging photoelectron photoion coincidence (i^{2}PEPICO) spectroscopy. In contrast to the photoelectron spectrum, the ground state TPES band exhibits a weak vibrational structure that correlates with strong peaks in the photoionization spectrum and is assigned to transitions to autoionizing Rydberg states converging to the ^{3}A″ cation state. While, at 8.462 eV, our calculations of the acetylene proton affinity confirm the vinyl adiabatic ionization energy from the ATcT, our experimental data agree with the literature photoelectron and photoionization spectra. The discrepancy is explained by negligible Franck–Condon factors for the origin transition from the bent Y-shaped neutral minimum to the bridge-shaped ionic minimum. We propose that the photoionization signal can instead be assigned in its entirety to three transitions: (i) straight Y-shaped $C_2H_3^{\ddagger}$ → bridged $C_2H_3^+$, (ii) straight Y-shaped $C_2H_3^{\ddagger}$ → straight Y-shaped $C_2H_3^+$ and (iii) bent Y-shaped C_2H_3 → straight Y-shaped $C_2H_3^+$, tentatively assigned to the observed photoionization onsets at 8.25, 8.43, and 8.60 eV, respectively.

1. Introduction

The vinyl radical ($H_2C{=}CH$) is involved in the high-temperature oxidation and pyrolysis processes in the combustion of numerous hydrocarbon fuels.[1,2] Together with its cation, it is also a common intermediate in plasma chemistry,[3] interstellar chemistry[4] and interstellar physics.[5] The ionization energy (IE) is characteristic of the feasibility of electron transfer and can indicate the likelihood of redox processes in chemistry and biology.[6] Yet, the computational as well as photoionization and photoelectron spectral IE determinations of the smallest alkenyl radical markedly disagree. The three key vinyl structures in the neutral and cationic state are shown in Fig. 1,[7] together with the highest (singly) occupied molecular orbital (SOMO) and SOMO−1 in the neutral, of which the latter corresponds to the HOMO of the vinyl cation. The neutral radical exhibits a doubly degenerate global minimum of a planar C_s structure (bent Y-shaped [**1**]). Experimental and theoretical studies on the tunneling splitting found that the minima are connected by a straight Y-shaped C_{2v} transition state, [**2**]‡, along the CCH bending mode. The electronic energy of this transition state has been reported to be about 0.21 eV above that of the global minimum in various experimental[8,9] and computational[10–14] works. After years of quantum chemical research, a consensus has emerged that, similarly to the ethyl cation,[15] the vinyl cation also has a non-classical C_{2v} global minimum with a proton bridging the two carbon atoms, [**3**]$^+$. A shallow local minimum also exists at a planar straight Y-shaped C_{2v} symmetric structure, [**2**]$^+$.[16–22] However, as we will show later, this consensus is somewhat troubled by the fact that lower-level theoretical approaches often give vastly different results.

In addition to the direct experimental measurements, thermochemical cycles and quantum chemical calculations[23,24] have been used to understand the neutral and cationic vinyl structure and energetics as well as to obtain the IE of the vinyl radical.[25] Harrison and Lossing[26] first reported IE(C_2H_3) = 9.45 eV by electron ionization (EI) measurements of pyrolytically prepared vinyl radicals from divinyl mercury in 1959. Later, Lossing[27] used an energy-resolved electron beam to re-measure IE(C_2H_3) at 8.95 eV using divinyl sulfone as a precursor. Berkowitz *et al.*[7] used photoionization spectra to measure the IE of the vinyl radical as prepared by fluorine abstraction from C_2H_4 and pyrolysis of divinyl mercury, respectively. Their observed ionization threshold was 8.59 ± 0.03 eV with the F atom reaction, and significantly lower, at 8.43 ± 0.03 eV, using pyrolysis. They interpreted the

[a] *Laboratory for Femtochemistry and Synchrotron Radiation, Paul Scherrer Institute, 5232 Villigen, Switzerland. E-mail: andras.boedi@psi.ch*

[b] *Hefei National Laboratory for Physical Sciences at the Microscale, Department of Chemical Physics, University of Science and Technology of China, Hefei 230026, China. E-mail: xzhou@ustc.edu.cn*

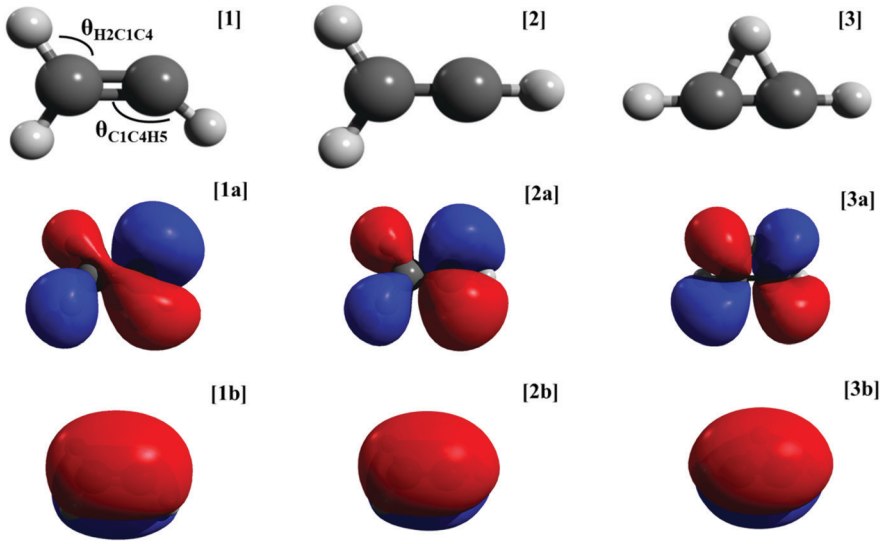

Fig. 1 Structures of the bent Y-shaped vinyl radical minimum [**1**], the straight Y-shaped transition state [**2**] and the bridge-shaped non-classical cationic minimum [**3**] together with the related SOMO [**1a**], [**2a**] and [**3a**] as well as SOMO−1 orbitals [**1b**], [**2b**] and [**3b**] of the neutral at these geometries. The latter also correspond to the HOMO of the cation state.

lower ionization onset in the pyrolysis experiment as a result of hot band transitions, due to higher sample temperature when compared with fluorine abstraction. They also observed a vibrational structure in the photoionization spectrum, which they proposed to be due to a Rydberg series converging to the excited $^3A''$ state of the vinyl cation. In fact, the photoelectron spectrum often provides an isomer-specific vibrational fingerprint and can even be used as an analytical tool.[28] But when Blush and Chen pyrolyzed *tert*-butyl peracrylate and studied the photoelectron spectrum of the vinyl radical,[29] they did not see any vibrational structure. However, on the basis of the onset of the spectrum and surmising that it is only negligibly red-shifted due to hot band transitions, they assigned IE(C_2H_3) as 8.25 ± 0.05 eV. Savee *et al.* produced the vinyl radical from methyl vinyl ketone and vinyl iodide photolytically, and reported photoionization spectra which agreed well with the F-abstraction results of Berkowitz *et al.* as well as absolute photoionization cross sections.[30] Fischer interpreted the discrepancy between the photoionization and photoelectron spectra as inconclusive evidence for the low-energy non-classical bridged structure of the vinyl radical.[31] Lau and Ng computed extrapolated wave function theory ionization energies for five hydrocarbon radicals, including the vinyl radical, for which they reported IE = 8.485 eV, seemingly confirming the photoionization onset measured with the pyrolysis source of Berkowitz *et al.*[24] This computational result is also in agreement with the Active Thermochemical Tables (ATcT), which yield IE(C_2H_3) = 8.477 ± 0.007 eV.[32–36] However, the ATcT vinyl cation enthalpy of formation is based predominantly on calculations as well as on dissociative photoionization thresholds for halogen loss from vinyl halogenides.[37–39] On the one hand, as we will show later, although increasingly accurate wave function approximation methods converge to the exact solution of the Schrödinger equation,[40] the optimized geometries and relative energies of the different vinyl cation isomers depend on the level of theory to a disconcerting degree. On the other hand, in the presence of reverse barriers, dissociative photoionization thresholds correspond to the transition state energy and not to the thermochemical threshold to halogen loss. As a large geometry change is required to yield the bridged structure $[3]^+$ from vinyl halogenide cations, there is no conclusive evidence whether this dissociation involves a reverse barrier. Because of the breadth of the underlying experimental and computational data as well as their interconnectedness, ATcT are the most trustworthy source of energetics data. However, the variance of the computational results as well as the contradictory photoionization and photoelectron spectra call for reconciliation in a holistic approach. As mentioned above, the vinyl radical undergoes rather large geometry change upon ionization and, in light of the latest computational results, it seems to be unlikely that the ionization cross-section is measureable at the adiabatic ionization energy. When the nuclear geometries of the neutral and the cation are different, this is quite often the case: because of methyl internal rotation upon ionization, the connection between some alkyl radical photoelectron spectra and their ionization energy was also discussed recently.[41] The ethanol ionization energy was reported to lie *ca.* 100 meV below the photoionization onset because of poor Franck–Condon overlap of the neutral and ionic minima.[42] The difference is even more extreme for adipic acid, for which the adiabatic ionization energy lies 1.5 eV below the onset of the TPES.[43] As seen in the case of HCO, a triatomic molecule undergoing large geometry change upon ionization, the adiabatic ionization energy may remain hidden even in the presence of vibrational fine structure. However, careful analysis and extrapolation of the vibrational structure allowed Dyke to determine the adiabatic ionization energy,[44] which was later confirmed by a double-resonance experiment by Mayer and Grant directly.[45] Yet the fact that the IE should lie significantly higher than the

ionization onset still remains to be explained. This motivated us to revisit the valence photoionization of the vinyl radical.

In this paper, we study the ionization of the vinyl radical by double imaging photoelectron photoion coincidence (i^2PEPICO) spectroscopy, which involves photoion mass analysis simultaneously with kinetic energy analysis of the coincident photoelectron. Thus, not only can we record photoionization spectra (sometimes incorrectly termed photoionization efficiency, PIE, curves) but also photoion mass-selected threshold photoelectron spectra (ms-TPES). By selecting mass channel 27, we can, for the first time, record the vinyl TPES without contributions of precursors or side products. Quantum chemical calculations support our experimental results, confirm the ionization energy of the vinyl radical and allow for new insights into the ionization pathways of the vinyl radical.

2. Experimental and computational

2.1 i^2PEPICO experiments

PEPICO experiments were performed at the VUV beamline of the Swiss Light Source, Paul Scherrer Institute, using a double imaging Photoelectron Photoion Coincidence (CRF-PEPICO) spectrometer. A detailed description of the beamline and the endstation can be found elsewhere,[46,47] and only a brief overview is given here. Synchrotron radiation was generated using a bending magnet, collimated, dispersed using a grazing incidence monochromator with a 150 lines per mm blazed grating, and focused into a gas filter. The gas filter was filled with a mixture of neon, argon and krypton at a pressure of 10 mbar to suppress higher order radiation above 14 eV effectively. The monochromatic VUV radiation crossed the sample beam orthogonally in the ionization chamber with a spot size of about 4×2 mm^2. The photon energy was calibrated using argon autoionization lines, recorded in first and second order of the grating, and the photon energy resolution was 5 meV at 8 eV.

The vinyl radical was prepared by flash pyrolysis of divinyl sulfone (DVS, Sigma-Aldrich, 97%). The precursor was kept at 313 K in a sample holder and seeded in argon from a backing pressure of *ca.* 800 mbar through a 100 μm nozzle into an in-vacuum, 1 mm internal diameter heated SiC microreactor, forming a continuous molecular beam at a concentration of *ca.* 0.25%. The heated microreactor was operated at a short residence time, estimated at *ca.* 100 μs based on the results of Guan *et al.*,[48] which allowed for efficient thermal decomposition and ensured the survival of elusive, unstable species, such as free radicals. In the interaction region, the VUV light crossed the sample beam and the resulting photoelectrons and photoions were extracted to opposite directions by a constant, 240 V cm^{-1}, electric field. The electrons and ions were velocity map imaged onto two Roentdek DLD40 position sensitive delay-line anode detectors. The electron time of flight (TOF) is negligible relative to the TOF of ions, thus the electron triggers the start signal for the ion TOF analysis.[49] The arrival times of the photoelectrons were correlated with that of the photoions to obtain the ion TOF distributions.

Threshold electrons (kinetic energy <5 meV) are imaged onto a central spot on the detector together with kinetic energy electrons with a negligible off-axis momentum component. The latter make up the hot electron contamination, which can be approximated based on a small ring around the center spot and subtracted as proposed by Sztáray and Baer.[50] Threshold photoelectrons detected in coincidence with a photoion at a certain time-of-flight can be selected and their intensity plotted as a function of the photon energy to yield the photoion mass-selected threshold photoelectron spectrum (ms-TPES).

2.2 Quantum chemical calculations

The geometry of the neutral vinyl radical was optimized using density functional theory (DFT) at the B3LYP/6-31G(2df,p) and B3LYP/cc-pVTZ+1d levels as well as by wave function theory (WFT) at the QCISD/6-311G(d,p) level of theory. The vertical ionization energy was calculated by evaluating the neutral and cation energies at the neutral geometry with the Gaussian-4 (G4),[51] W1U,[52] and CBS–APNO[53] methods, respectively. The ionization energies to the two vinyl cation isomers ($[\mathbf{1}] \rightarrow [\mathbf{2}]^+$ and $[\mathbf{1}] \rightarrow [\mathbf{3}]^+$) were calculated using these composite methods, as well. The interconversion path for $[\mathbf{2}]^+ \rightarrow [\mathbf{3}]^+$ was calculated at the Hartree–Fock, frozen-core second order perturbation theory (MP2) and frozen-core coupled cluster singles and doubles (CCSD) level using the def2-TZVPP basis set. We also optimized the isomerization path using all electron MP2 with the aug-cc-pCVTZ basis set. In addition to B3LYP/6-311++G(d,p) calculations, the DFT functionals M06-2X and ωB97X-D were also used with the def2-TZVPP basis set. Lastly, the electronic energy was also evaluated using the CBS–APNO and W1U methods along the CCSD/def2-TZVPP path. As it appeared to be the most reliable among the computationally efficient methods (see below), we used M06-2X/def2-TZVPP to explore the potential energy surface (PES) of the neutral vinyl in the electronic ground state and that of the cation in the ground and the first triplet electronic states along the bond angles, θ_{C1C4H5} and θ_{H2C1C4}. All calculations were performed using the Gaussian 16 program package using unrestricted reference functions for open-shell calculations.[54]

3. Results and discussion

3.1 Photoionization time-of-flight mass spectra

Photoionization TOF mass spectra of DVS recorded at two photon energies, 9.00 and 12.70 eV, are shown in Fig. 2. No ions were observed in the mass spectrum without pyrolysis (Fig. 2a) at 9.00 eV, *i.e.*, below the adiabatic ionization energy of DVS, 10.56 eV.[55] At 12.70 eV, dissociative photoionization fragment ions of DVS appeared, *e.g.*, at m/z 41 ($C_3H_5^+$ or C_2HO^+), 59 ($C_2H_3O_2^+$ or $C_2H_3S^+$), 60 ($C_2H_4O_2^+$ or $C_2H_4S^+$), 69 ($C_4H_5O^+$) and 75 ($C_2H_3OS^+$). The DVS parent ion at m/z 118 is rather unstable and barely detectable in the spectrum. The vinyl ion at m/z 27 ($C_2H_3^+$) was only observed as a dissociative photoionization product in small quantities above 13.30 eV without pyrolysis. Thus, the dissociative photoionization of the

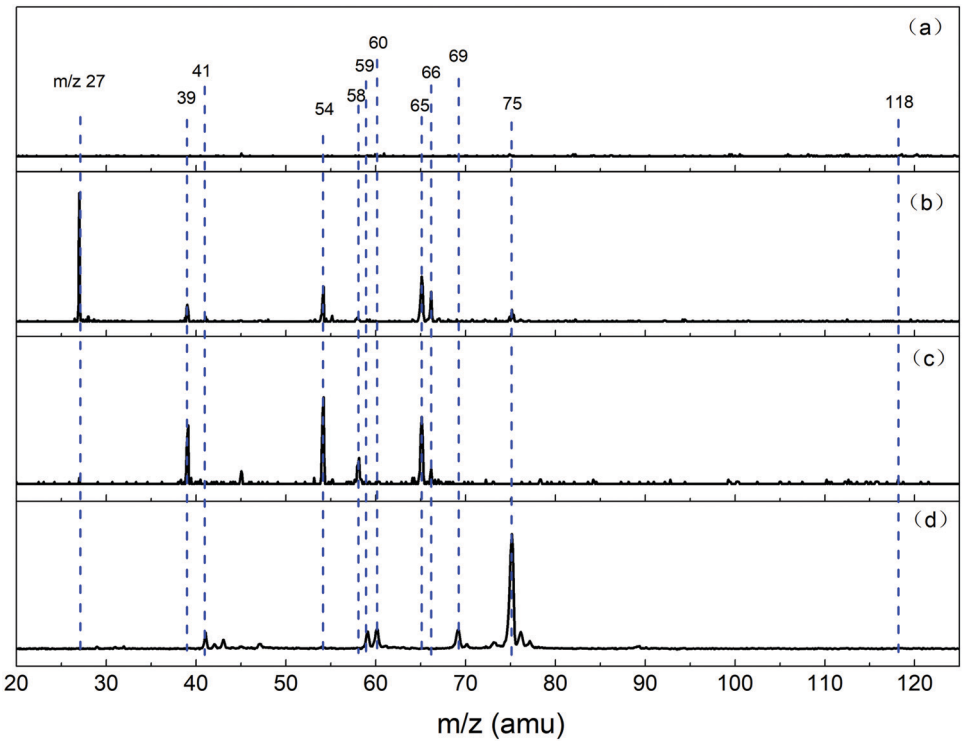

Fig. 2 TOF mass spectra of DVS recorded at (a) 9.00 eV without pyrolysis, (b) 9.00 eV with a pyrolysis power of 35 W, (c) 9.00 eV with a pyrolysis power of 46 W, and (d) 12.70 eV without pyrolysis.

precursor does not interfere with the vinyl signal in the energy range studied herein.

When the flash pyrolysis source was heated, several peaks were newly observed in the mass spectra (Fig. 2b and c), such as *m*/*z* 27 ($C_2H_3^+$, vinyl radical), 39 (C_3H_3, *e.g.*, propargyl radical), 54 (C_4H_6, *e.g.*, 1,3-butadiene), 65 (C_5H_5, *e.g.*, cyclopentadienyl radical), and 66 (C_5H_6, *e.g.*, cyclopentadiene).[56] These peaks are distinct from the ones due to dissociative photoionization of DVS (Fig. 2d), and, at a low photon energy of 9 eV, are the products of direct photoionization of the corresponding neutrals, indicative of bimolecular chemistry occurring in the pyrolysis reactor. The bimolecular products are formed in exothermic reactions and have dissociative ionization thresholds above that of the precursor DVS. They are also unlikely to form the vinyl cation as a fragment ion in the studied energy range. Therefore, and thanks to photoion mass selection, the *m*/*z* 27 ms-TPES is entirely due to the vinyl radical TPES. The pyrolysis power was optimized to 35 W (corresponding to an outer reactor temperature of *ca.* 800 °C, Fig. 2b) so that the intensity of *m*/*z* 27 peak was at a maximum. Upon increasing the temperature further, the vinyl peak almost vanished at a power of 46 W (*ca.* 950 °C, Fig. 2c). We attribute this decrease to sequential hydrogen loss from vinyl to yield acetylene, which remains unionized at 9 eV.

3.2 Photoionization spectrum

The photoionization spectrum of the vinyl radical at *m*/*z* 27 showed an excellent signal-to-noise ratio as seen in Fig. 3 together with the spectrum of Berkowitz *et al.* obtained with

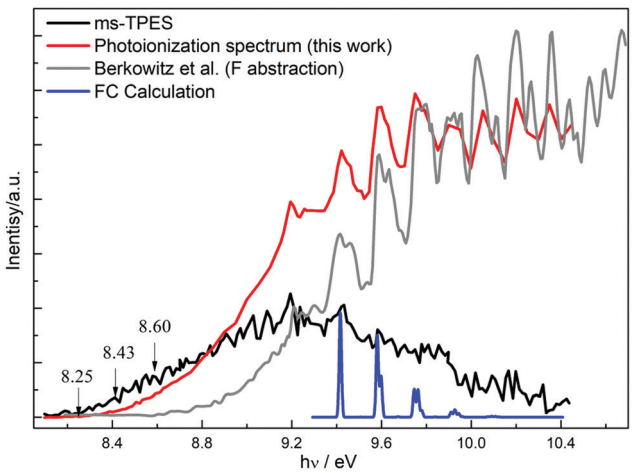

Fig. 3 Photoionization (red) and mass-selected threshold photoelectron spectrum (black) of the vinyl radical. Also shown is a Franck–Condon simulation to the first triplet state, shifted to 9.42 eV (blue) and the photoionization spectrum of the cold vinyl radical produced in the F + C_2H_4 reaction (gray).[7]

fluorine abstraction.[7] A strong progression starts at *ca.* 9.20 eV, which is evident in all previously recorded photoionization spectra but not seen in the photoelectron spectrum of Blush and Chen.[29] This indicates a transition to a neutral state, which is only resonant at the corresponding photon energy, and yields photoelectrons by rovibrational autoionization to the electronic ground $^1A'$ cation state below. Such vibrational progressions are expected for Rydberg manifolds corresponding to ions with

a similar geometry to the neutral. Indeed, as will be shown later, the potential energy surface of the $^3A''$ cation state, at a M06-2X calculated electronic ionization energy of 10.41 eV (*cf.* the zero-point corrected W1U result of 10.75 eV), resembles that of the neutral. Based on the molecular orbital structure (Fig. 1), it is likely that the singlet excited state $^1A''$ behaves similarly to this triplet state, but time-dependent DFT calculations failed to converge to a meaningful root. Nevertheless, we could obtain a good fit to the measured vibrational progression by shifting the origin of the Franck–Condon simulation of the triplet spectrum to 9.42 eV (see Fig. 3). This was done on the basis of the origin transition being the strongest one in the calculation and assuming that the weak shoulder at 9.20 eV corresponds to a hot band. A doublet structure is more evident in the spectrum of Blush and Berkowitz, recorded at a smaller step size than herein, and the simulation also predicts two vibrations, the C–C stretching and CH_2 bending modes to be active at 1328 and 1464 cm^{-1}, respectively. However, as the doublet is seen already in the first band, it is also possible that it is due to resonant excitation to two, slightly different Rydberg series. Furthermore, the intensity of the autoionization progression is approximately constant, whereas the Franck–Condon factors are calculated to drop quickly in the spectrum. This can be due to drastically increased autoionization cross sections for higher lying vibrational states or also to the fact that we observe the superposition of more than one Rydberg state.

Berkowitz *et al.* utilized fluorine abstraction from ethylene and pyrolysis of the divinyl mercury precursor to prepare the vinyl radical.[7] The photoionization spectrum shown in Fig. 3 corresponds to the former, which yielded an ionization onset of 8.59 ± 0.03 eV. They reported the ionization onset as 8.43 ± 0.03 eV using pyrolysis explaining the difference by the presence of hot bands in the pyrolysis spectrum. When modeling the onset energy range of the photoionization spectrum, we can also extrapolate the photoionization spectrum from 8.5 to 8.7 eV back to an onset at 8.43 eV, although we used a different precursor, DVS (see below). The suboptimal expansion from the SiC microreactor only leads to limited rovibrational cooling, as was shown by the estimated 550 K rovibrational temperature for the methyl radical post-expansion at a pyrolysis temperature of about 1100 K in a similar setup.[57] Threshold photoionization PEPICO breakdown diagrams can be used to measure the effective temperature of radical intermediates accurately, as was recently shown for the methyl peroxy radical.[58] However, the vinyl cation is stable, and hydrogen atom loss is only expected to take place 4.4 eV above the ionization energy.[32] Therefore, we only speculate that it is unlikely that our pyrolysis spectrum should correspond to the same vinyl radical effective temperature as in the Berkowitz experiment. Instead, it is more likely that the 8.43 eV photoionization spectrum onset is due to transitions from parts of the potential energy surface which only have significantly non-zero nuclear wave function in the hot source. As will be discussed in more detail later, a likely candidate for this onset is hot band transitions from the straight Y-shaped transition state $[\mathbf{2}]^{\ddagger}$ region in the neutral to the classical (straight Y-shaped) cation structure $[\mathbf{2}]^{+}$, which corresponds to a shallow local minimum on the ground singlet state cation potential energy surface.

3.3 Photoion mass-selected TPES

The ms-TPES of the vinyl radical exhibits a broad band in the energy range of 8.10–10.45 eV (Fig. 3). Our calculated triplet ionization at 10.75 eV as well as the first singlet excited state at *ca.* 11.2 eV[59] lie significantly higher in energy. Therefore, the whole band is attributed to the ground electronic $^1A'$ state of the vinyl cation. The TPES onset appears at 8.25 eV, in perfect agreement with the previous, fixed photon energy photoelectron spectrum.[29] As Blush and Chen recorded the spectrum without mass selection, to which higher IE pyrolysis co- and by-products also contributed above the onset, they could not identify the vertical IE of the vinyl radical. Instead, their time-of-flight photoelectron spectrum shows a high plateau starting at *ca.* 9.3 eV electron binding energy.[29] As conventionally assigned, the vertical ionization energy corresponds to the band maximum, as seen in the mass-selected TPES at 9.25 eV. We have looked into the meaning of vertical ionization beyond this assumption. Its IUPAC definition as an ionization process without a change in the position and momenta of the atoms[60] is questionable, because it rules out a change in the vibrational state. The maximum Franck–Condon overlap and the maximum signal intensity often involve a change in the vibrational state, hence in the momenta of the atoms. Therefore, the definition of the vertical ionization energy found in Wikipedia, *i.e.*, the energy difference at the maximum nuclear wave function overlap between the neutral and the ion, appears to be more appropriate.[61] As evidenced by the large and presumably temperature-dependent change in the photoionization spectrum observed by Berkowitz *et al.*,[7] the band maximum of the photoelectron spectrum (normally reported as the vertical ionization energy) may also be strongly temperature dependent. We also calculated the vertical ionization energy at the optimized neutral geometry, and found it to be *ca.* 9.59 eV (*vide infra*), indicating that band maximum at 9.25 eV is dominated by threshold ionization of vibrationally excited neutrals.

Upon closer inspection, the progression clearly seen in the literature as well as in the newly acquired photoionization spectra can also be observed in the threshold photoelectron spectrum, in particular the presumed hot-band transition and the two peaks thereafter. This is in contrast to the photoelectron spectrum of Blush and Chen, who reported a smooth Franck–Condon envelope with no fine structure. This provides further evidence to the ionization mechanism: intermediate Rydberg states are prepared when the photon energy is resonant with neutral energy levels and may autoionize to yield electrons with varying kinetic energy, including threshold electrons. However, most electrons will have non-zero kinetic energy and these events will only contribute to the total photoionization signal and not to the threshold photoelectron spectrum. As Blush and Chen used constant, 10.49 eV energy photons to record the spectrum, they could not observe such autoionizing progressions in the photoelectron spectrum.

Modeling vibrational progressions in the photoelectron spectrum allows for the assignment of complex spectra with multiple overlapping electronic states.[62] In the absence of a fine structure, the onset of the photoelectron spectrum is, however, not necessarily indicative of the ionization energy. If the geometry change upon ionization is large, a potentially significant excess energy may be needed to achieve measurable Franck–Condon overlap between the neutral and the cation states.[42,43] If a single, well-understood large-amplitude motion, *e.g.*, internal rotation, dominates the anharmonicity, the measured Franck–Condon envelope can still be used to extrapolate to the adiabatic ionization energy.[58] However, as indicated by previous computational results and confirmed below by the potential energy surface calculations, the geometry relaxation upon ionization of the vinyl radical is dominated by non-trivial large-amplitude motions to yield the non-classical bridged structure. Therefore, and because of the poorly defined internal temperature of the radicals, Franck–Condon simulation of the ground state band is not within reach. The potential energy surface can instead be explored to try to identify the dominant photoionization transitions and reconcile the apparently contradictory photoionization and photoelectron spectra.

3.4 Potential energy surfaces: structures, transitions and energetics

Calculations have established a single, doubly degenerate bent Y-shaped minimum for the neutral vinyl radical [**1**].[10,11] The singly occupied HOMO has some C–C anti-bonding character, and the C=C bond contracts upon ionization to the ^{1}A′ state. All established levels of theory agree that the lone hydrogen atom has an *ca.* 137° C=C–H bond angle in the bent Y-shaped neutral minimum [**1**]. Most methods agree that a cationic minimum exists, in which this bond becomes linear in the straight Y-shaped cationic isomer $[\mathbf{2}]^+$. The non-classical cation minimum consists of a quasi-linear H–C=C–H moiety, bridged by the third hydrogen atom at a C–H–C bond angle of *ca.* 62°, $[\mathbf{3}]^+$.

The neutral isomerization coordinate between the degenerate minima[10,11] and the ionic pathway between the classical and non-classical isomers[21,22] have both been studied computationally. We have found that the latter strongly depends on the level of theory used. As shown in Fig. 4, the classical minimum $[\mathbf{2}]^+$ is the global one at the Hartree–Fock level of theory, and the B3LYP functional predicts the two minima to be virtually isoenergetic with a significant interconversion barrier. Wave function theory methods including electron correlation agree that the non-classical structure $[\mathbf{3}]^+$ is significantly more stable than $[\mathbf{2}]^+$. Second order perturbation theory with or without a core correlation in fact predicts that the straight Y-shaped classical structure $[\mathbf{2}]^+$ is a transition state. The most trustworthy approaches, *i.e.*, the coupled-cluster results as well as the W1U and CBS–APNO energy profiles along the coupled cluster interconversion path agree that a small barrier separates the two minima. Among the density functional approaches, the M06-2X functional reproduces the high-level WFT results best. Therefore, we used the M06-2X/def2-TZVPP level of theory to

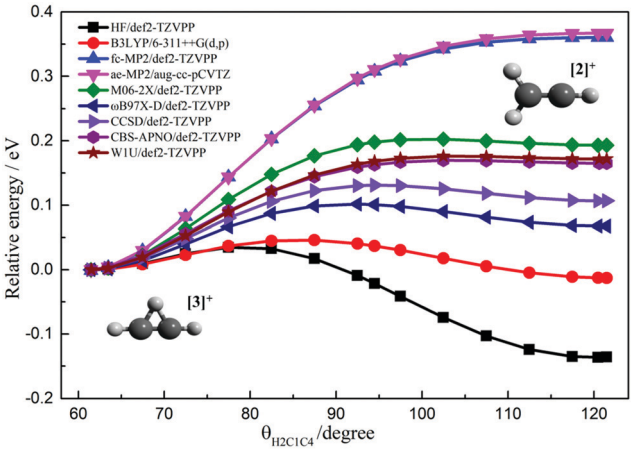

Fig. 4 Potential energy curves for the interconversion path from the non-classical cation bridged structure $[\mathbf{3}]^+$ to the straight Y-shaped structure $[\mathbf{2}]^+$, relative to the energy of $[\mathbf{3}]^+$. The single-point composite method energies for CBS-APNO and W1U have been evaluated along the coupled cluster path.

calculate the vinyl radical potential energy surface in the neutral ground ^{2}A′ as well as the ionic singlet ^{1}A′ and triplet ^{3}A″ electronic states as a function of bond angles θ_{C1C4H5} and θ_{H2C1C4} (Fig. 5, see Fig. 1 for the bond angle definitions). Along the former bond angle, *i.e.*, the bottom right axis, the straight [**2**] and bent [**1**] Y-shaped structures are connected. Along the latter bond angle, *i.e.*, the bottom left axis, the straight Y-shaped and the non-classical bridged structures [**3**] are connected. Thus, the important stationary points in the neutral and in the cation are all found in Fig. 5. On the one hand, the electronic energy of the barrier between the bent Y-shaped global minimum of the vinyl radical to the straight Y-shaped transition state is quite small, *ca.* 0.22 eV. On the other hand, the most energetic point on the neutral doublet PES is at the bridged-shaped structure at 2.43 eV.

The PES of the triplet state of the vinyl cation closely resembles that of the neutral ground state, which explains the success of the Franck–Condon simulation of the spectrum. This confirms that the autoionization progression observed primarily in the photoionization spectrum may belong to Rydberg states of the first triplet state of the vinyl cation. The dissimilarity between the potential energy surface of the singlet cation and the neutral ground state explains the surprisingly large intensity of the autoionization progression. Franck–Condon factors for ionization into the ground cation state are expected to be small and the autoionization signal can thus show up as a strong resonance.

The singlet vinyl cation's global minimum is the non-classical bridged structure $[\mathbf{3}]^+$ and the M06-2X/def2-TZVPP PES calculation also reproduces the straight Y-shaped local minimum $[\mathbf{2}]^+$, connected to the bridged-structure *via* a small barrier (Fig. 4 and 5b). This minimum is similar to the low-lying straight Y-shaped isomerization transition state $[\mathbf{2}]^‡$ of the vinyl radical, which yields favorable Franck–Condon factors for ionization in this range of the PES. The bent Y-shaped structure,

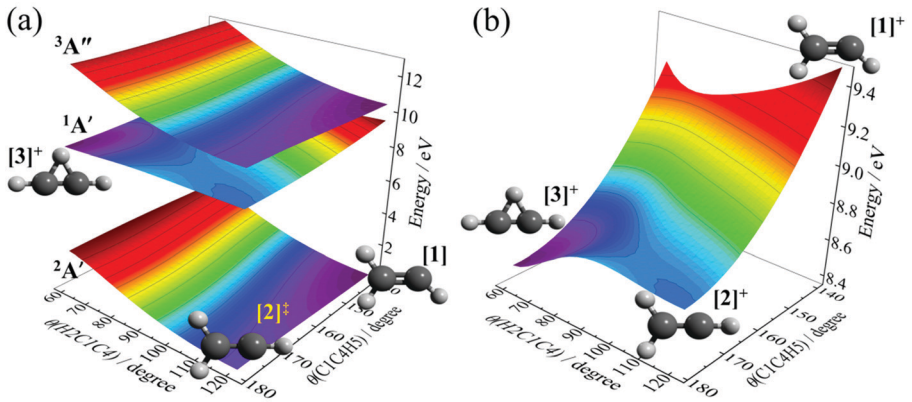

Fig. 5 (a) Vinyl PES at the M06-2X/def2-TZVPP level of theory in the neutral ground ^{2}A′ and cationic ^{1}A′ ground and first triplet ^{3}A″ electronic states along the bond angles θ_{C1C4H5} and θ_{H2C1C4}, (b) Zoom of the vinyl cation ground electronic state PES.

corresponding to the minimum on the neutral surface, is the highest energy region on the explored cation PES of the ^{1}A′ state.

The PES confirms that the origin transition between the neutral vinyl radical and the non-classical cationic minimum is inaccessible by photoionization, because the cationic global minimum corresponds to a high-energy maximum in the neutral. Therefore, efforts to determine the adiabatic ionization energy based on single-photon photoionization experiments are likely futile. Nevertheless, although the photoionization spectrum of the vinyl radical monotonically rises at the lowest energies, it still suggests a somewhat structured onset as seen in the zoomed plot of the 8.10–9.10 eV photon energy range in Fig. 6(a). The corresponding features are also expected to arise in the TPES but are not seen due to the worse signal-to-noise ratio there. We were interested to see if this structure can correspond to Franck–Condon allowed transitions. As the vinyl TPES signal is also contained in the photoionization signal, it is not surprising that the first, gradual rise is visible already at around 8.25 eV. This onset remained unassigned in the previous photoionization spectra probably because of an insufficient signal-to-noise ratio. Thereafter, the slope increases and the steeper range can be extrapolated to zero at *ca.* 8.43 eV similar to the pyrolysis experiment of Berkowitz *et al.*[7] A further, third contribution can be derived at around 8.60 eV, only slightly higher in energy than the reported 8.59 eV ionization onset with the cooler, fluorine abstraction vinyl source.[7] Thus, it appears that the previously reported thresholds are all contained in the pyrolysis photoionization spectrum.

In the pyrolysis experiments, C_2H_3 radicals are produced in a high-temperature SiC microreactor, and are only slightly cooled in the expansion. Because of the steeply increasing density of states, energy levels at the inversion transition state, *i.e.*, *ca.* 0.2 eV above the minimum, will have significant population. While the wave function of these states will still be predominantly localized above the double potential energy well, it will not vanish in the vicinity of $[\mathbf{2}]^‡$. The nuclear wave function overlap with the Y-shaped ionic minimum is much enhanced in this region, which may therefore be the source of the bulk of the ionization signal. Generally speaking, the two minima on the cation surface, namely the straight Y-shaped $[\mathbf{2}]^+$ and the non-classical bridged structure $[\mathbf{3}]^+$ are candidates for the final state at lower energies, as the bent Y-shaped ion structure $[\mathbf{1}]^{+‡}$ is exceedingly high in energy. As shown in Fig. 6(b), the transitions between these structures are calculated to be at energies representative of the onset structure of the photoionization spectrum: the ionization energy from [**1**] to $[\mathbf{2}]^+$ is expected to be the main contributor to the photoionization spectrum of cold vinyl radicals, and is computed to lie at

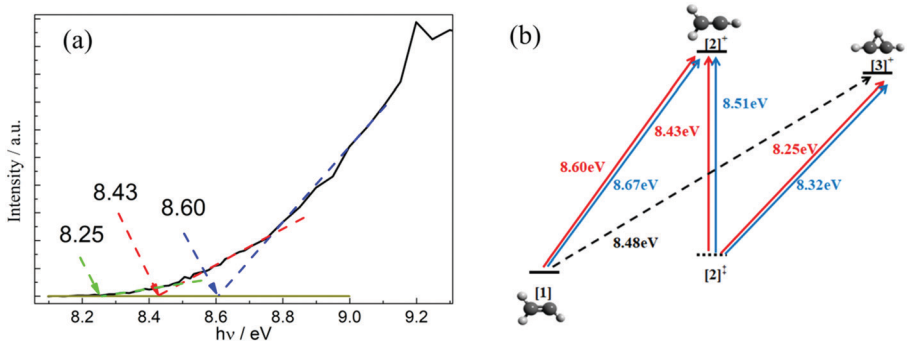

Fig. 6 (a) Magnified view of the vinyl photoionization spectrum between 8.10 and 9.25 eV. (b) Schematic diagram of vinyl radical ionization channels, shown with calculated ionization energies (blue) and the experimentally observed onsets (red). The black dashed line corresponds to adiabatic ionization, which is not observed in the experiment.

8.68 eV. The hot band transition from the transition state region of $[\mathbf{2}]^{\ddagger}$ to $[\mathbf{2}]^{+}$ has a computed minimum energy of 8.46 eV, and is expected to be Franck–Condon allowed if the neutral sample is hot enough to have non-vanishing nuclear wave function in this range of the PES. Indeed, this transition dominates the pyrolysis photoionization spectra. Lastly, we may expect limited Franck–Condon activity from non-zero nuclear wave functions in the transition state region to the global non-classical minimum of the cation, since the two are connected by a single C=C–H bend mode. The calculated 8.25 eV agrees exactly with the ionization onset observed in pyrolysis experiments by photoelectron spectroscopy and also in the photoionization spectrum herein. In addition to the M06-2X electronic energies, we also calculated the ionization energies between these stationary points including the zero-point energy correction using the G4, W1U, and CBS–APNO composite methods, and the average values are displayed in Fig. 6(b). Although the agreement between the onset of these, theoretically possible processes and the photoionization spectral structure may well be coincidental, we still find it reassuring that the tentative fine structure of the photoionization spectrum can be reproduced by such a crude model quite well, based only on qualitative consideration of neutral populations and nuclear wave function overlap integrals.

The Franck–Condon factors for these transitions are still likely to be rather small. In addition to the large intensity of autoionization resonances, this also explains the structure and temperature-dependence of the spectrum. Ionizing transitions from the bottom of the vinyl potential energy well are extremely unlikely and the Franck–Condon factors grow progressively for the hot bands as the neutral internal energy is increased. However, the population drops precipitously especially at lower temperatures. The spectrum is the result of the interplay between a steeply increasing (Franck–Condon factors of progressive hot bands) and a steeply decreasing (Boltzmann distribution) function of internal energy, and is very sensitive to the latter.

The vertical ionization energy can also be approximated as the difference between the cation and neutral electronic energy at the optimized neutral minimum. For the vinyl radical, the average computed vertical ionization is 9.59 eV at the G4, CBS–APNO, and W1U levels of theory, much higher than the observed 9.25 eV TPES band maximum. The reason for this difference is the sharply increasing Franck–Condon factors as a function of neutral internal energy and the rovibrationally hot pyrolysis vinyl source. Thus, not only is photoionization the wrong method to measure the adiabatic ionization energy, even the vertical ionization energy (if defined temperature independently as the transition from the vibrational ground state of the neutral to the vibrational state with maximum nuclear wave function overlap of the cation) is hidden from sight in the photoelectron spectra.

We also applied a combined experimental–theoretical approach to calculate the adiabatic ionization energy of the vinyl radical. As mentioned earlier, the Active Thermochemical Tables yield 8.477 ± 0.007 eV for this quantity, whereby, in the provenance analysis, the vinyl cation enthalpy of formation at 1119.15 ± 0.59 kJ mol^{-1} is dominated by the measured dissociative photoionization threshold of vinyl chloride.[39] This value may be affected by a small reverse barrier, leading to a vinyl ionization energy that is too high. The Active Thermochemical Tables also report a very accurate ethylene proton affinity at 674.04 ± 0.33 kJ mol^{-1}. We calculated the proton affinity of acetylene and ethylene using the G4, CBS–APNO and W1U methods, and corrected the calculated acetylene proton affinity using the computed error in the ethylene proton affinity at the respective level of theory. Based on the ATcT vinyl enthalpy of formation, $\Delta_f H^{\ominus}_{0\,K}(C_2H_2)$ = 228.82 ± 0.13 kJ mol^{-1}, the thus derived heat of formation of the vinyl cation, we arrive at a vinyl ionization energy of 8.462, which is probably accurate to within 20 meV and only barely lower than the ATcT value of 8.477 ± 0.007 eV.

4. Conclusions

VUV synchrotron radiation and double imaging photoelectron photoion coincidence spectroscopy has been used to investigate the photoionization of vinyl radicals prepared by flash pyrolysis. The photoionization spectrum of the vinyl radical agreed with the literature result and exhibited a strong autoionization progression. Traces of this were also visible in the mass-selected threshold photoelectron spectrum (ms-TPES), which agreed with the photoelectron spectrum otherwise. Based on the spectra, the comparison with the literature and a M06-2X-calculated potential energy surface, we propose that there are three onsets in the photoionization spectrum at *ca.* 8.25, 8.43, and 8.60 eV. These correspond to the $[\mathbf{2}]^{\ddagger} \rightarrow [\mathbf{3}]^{+} + e^{-}$, $[\mathbf{2}]^{\ddagger} \rightarrow [\mathbf{2}]^{+} + e^{-}$, and $[\mathbf{1}] \rightarrow [\mathbf{2}]^{+} + e^{-}$ ionization processes (see Fig. 1 for structures), respectively, and none is related to the adiabatic ionization of $[\mathbf{1}] \rightarrow [\mathbf{3}]^{+} + e^{-}$. The strong temperature-dependence of the photoionization spectrum is due to the interplay between the steeply rising Franck–Condon factors and the precipitously falling neutral population with increasing internal energy. This also gives rise to an uncharacteristically low ionization onset, *ca.* 0.2 eV below the adiabatic ionization energy, and to a strong autoionization progression in the photoionization spectrum. Thus, the adiabatic ionization energy of the vinyl radical cannot be directly measured, only calculated or established by thermochemical cycles. Literature extrapolated WFT results, the Active Thermochemical Tables and our ATcT-corrected composite method approach agree that IE(C_2H_3) is 8.485, 8.477 ± 0.007, and 8.462 eV, respectively. We also point out the significant differences between WFT and DFT results for the singlet cation potential energy surface, which may have misled experimenters in the past, as well as the ambiguous definition of the vertical ionization energy in the literature. Finally, we conclude that the apparent contradiction between historical experimental results and more contemporary calculations only arose because of attempts to measure and assign the adiabatic energy with the help of spectra that are independent of it.

Conflicts of interest

There are no conflicts of interest to declare.

Acknowledgements

The experimental work was carried out at the VUV beamline of the Swiss Light Source of the Paul Scherrer Institute. The financial support from the Swiss Federal Office for Energy (BFE Contract No. SI/501269-01) and the National Natural Science Foundation of China (No. 21573210 and 21873089) is gratefully acknowledged. This work was also financially supported by the National Key Research and Development Program of China (No. 2016YFF0200502) and the National Key Basic Research Foundation of China (No. 2013CB834602). X. Wu appreciates the Chinese Postdoctoral Foundation (No. 2018M632535) and the USTC-NSRL Association for support too.

References

1 P. R. Westmoreland, A. M. Dean, J. B. Howard and J. P. Longwell, *J. Phys. Chem.*, 1989, **93**, 8171–8180.
2 J. A. Miller, R. J. Kee and C. K. Westbrook, *Annu. Rev. Phys. Chem.*, 1990, **41**, 345–387.
3 R. Janev and D. Reiter, *Phys. Plasmas*, 2004, **11**, 780–829.
4 A. Fahr, P. S. Monks, L. J. Stief and A. H. Laufer, *Icarus*, 1995, **116**, 415–422.
5 A. Glassgold, A. Omont and M. Guelin, *Astrophys. J.*, 1992, **396**, 115–119.
6 C.-Y. Ng, T. Baer and I. Powis, *Unimolecular and bimolecular ion-molecule reaction dynamics*, Wiley, 1994.
7 J. Berkowitz, C. Mayhew and B. Ruščić, *J. Chem. Phys.*, 1988, **88**, 7396–7404.
8 H. Kanamori, Y. Endo and E. Hirota, *J. Chem. Phys.*, 1990, **92**, 197–205.
9 K. Tanaka, M. Toshimitsu, K. Harada and T. Tanaka, *J. Chem. Phys.*, 2004, **120**, 3604–3618.
10 D. J. Nesbitt and F. Dong, *Phys. Chem. Chem. Phys.*, 2008, **10**, 2113–2122.
11 A. R. Sharma, B. J. Braams, S. Carter, B. C. Shepler and J. M. Bowman, *J. Chem. Phys.*, 2009, **130**, 174301.
12 L. Chen, K. Shao, J. Chen, M. Yang and D. H. Zhang, *J. Chem. Phys.*, 2016, **144**, 194309.
13 H.-G. Yu, H. Song and M. Yang, *J. Chem. Phys.*, 2017, **146**, 224307.
14 J. Šmydke, C. Fábri, J. Sarka and A. G. Császár, *Phys. Chem. Chem. Phys.*, 2019, **21**, 3453–3472.
15 B. Ruscic, J. Berkowitz, L. Curtiss and J. Pople, *J. Chem. Phys.*, 1989, **91**, 114–121.
16 M. W. Crofton, M. F. Jagod, B. D. Rehfuss and T. Oka, *J. Chem. Phys.*, 1989, **91**, 5139–5153.
17 L. Knoll, Z. Vager and D. Marx, *Phys. Rev. A: At., Mol., Opt. Phys.*, 2003, **67**, 022506.
18 J. Li, A. B. Pacheco, K. Raghavachari and S. S. Iyengar, *Phys. Chem. Chem. Phys.*, 2016, **18**, 29395–29411.
19 C. Liang, T. P. Hamilton and H. F. Schaefer III, *J. Chem. Phys.*, 1990, **92**, 3653–3658.
20 D. Marx and M. Parrinello, *Science*, 1996, **271**, 179–181.
21 A. R. Sharma, J. Wu, B. J. Braams, S. Carter, R. Schneider, B. Shepler and J. M. Bowman, *J. Chem. Phys.*, 2006, **125**, 224306.
22 B. T. Psciuk, V. A. Benderskii and H. B. Schlegel, *Theor. Chem. Acc.*, 2007, **118**, 75–80.
23 M. N. Glukhovtsev and R. D. Bach, *Chem. Phys. Lett.*, 1998, **286**, 51–55.
24 K.-C. Lau and C. Ng, *J. Chem. Phys.*, 2005, **122**, 224310.
25 X. Qian, K. Lau and C. Ng, *J. Chem. Phys.*, 2004, **120**, 11031–11041.
26 A. Harrison and F. Lossing, *J. Am. Chem. Soc.*, 1960, **82**, 519–521.
27 F. Lossing, *Can. J. Chem.*, 1971, **49**, 357–362.
28 A. Bodi, P. Hemberger, D. L. Osborn and B. l. Sztáray, *J. Phys. Chem. Lett.*, 2013, **4**, 2948–2952.
29 J. A. Blush and P. Chen, *J. Phys. Chem.*, 1992, **96**, 4138–4140.
30 J. D. Savee, J. F. Lockyear, S. Borkar, A. J. Eskola, O. Welz, C. A. Taatjes and D. L. Osborn, *J. Chem. Phys.*, 2013, **139**, 056101.
31 I. Fischer, *Int. J. Mass Spectrom.*, 2002, **216**, 131–153.
32 B. Ruscic and D. H. Bross, in *available at ATcT.anl.gov*, 2019.
33 B. Ruscic, R. E. Pinzon, M. L. Morton, G. von Laszevski, S. J. Bittner, S. G. Nijsure, K. A. Amin, M. Minkoff and A. F. Wagner, *J. Phys. Chem. A*, 2004, **108**, 9979–9997.
34 B. Ruscic, R. E. Pinzon, G. Von Laszewski, D. Kodeboyina, A. Burcat, D. Leahy, D. Montoy and A. F. Wagner, *J. Phys.: Conf. Ser.*, 2005, **16**, 561–570.
35 B. Ruscic, *Int. J. Quantum Chem.*, 2014, **114**, 1097–1101.
36 B. Ruscic, *J. Phys. Chem. A*, 2015, **119**, 7810–7837.
37 L. Sheng, F. Qi, L. Tao, Y. Zhang, S. Yu, C.-K. Wong and W.-K. Li, *Int. J. Mass Spectrom. Ion Processes*, 1995, **148**, 179–189.
38 K.-C. Lau and C.-Y. Ng, *Acc. Chem. Res.*, 2006, **39**, 823–829.
39 N. S. Shuman, M. A. Ochieng, B. Sztáray and T. Baer, *J. Phys. Chem. A*, 2008, **112**, 5647–5652.
40 H. Chung, B. Braams, K. Bartschat, A. Császár, G. Drake, T. Kirchner, V. Kokoouline and J. Tennyson, *J. Phys. D: Appl. Phys.*, 2016, **49**, 363002.
41 F. Holzmeier, M.-P. Herbert, I. Fischer, M. Steglich, A. Bodi and P. Hemberger, *J. Anal. Appl. Pyrolysis*, 2017, **124**, 454–460.
42 A. Bodi, M. D. Brannock, B. Sztáray and T. Baer, *Phys. Chem. Chem. Phys.*, 2012, **14**, 16047–16054.
43 M. F. Heringa, J. G. Slowik, A. S. Prévôt, U. Baltensperger, P. Hemberger and A. Bodi, *J. Phys. Chem. A*, 2016, **120**, 3397–3405.
44 J. M. Dyke, *J. Chem. Soc., Faraday Trans. 2*, 1987, **83**, 69–87.
45 E. Mayer and E. R. Grant, *J. Chem. Phys.*, 1995, **103**, 10513–10519.
46 M. Johnson, A. Bodi, L. Schulz and T. Gerber, *Nucl. Instrum. Methods Phys. Res., Sect. A*, 2009, **610**, 597–603.
47 B. Sztáray, K. Voronova, K. G. Torma, K. J. Covert, A. Bodi, P. Hemberger, T. Gerber and D. L. Osborn, *J. Chem. Phys.*, 2017, **147**, 013944.
48 Q. Guan, K. N. Urness, T. K. Ormond, D. E. David, G. Barney Ellison and J. W. Daily, *Int. Rev. Phys. Chem.*, 2014, **33**, 447–487.
49 A. Bodi, B. Sztáray, T. Baer, M. Johnson and T. Gerber, *Rev. Sci. Instrum.*, 2007, **78**, 084102.
50 B. Sztáray and T. Baer, *Rev. Sci. Instrum.*, 2003, **74**, 3763–3768.
51 L. A. Curtiss, P. C. Redfern and K. Raghavachari, *J. Chem. Phys.*, 2007, **126**, 084108.

52 E. C. Barnes, G. A. Petersson, J. A. Montgomery Jr, M. J. Frisch and J. M. Martin, *J. Chem. Theory Comput.*, 2009, **5**, 2687–2693.
53 J. W. Ochterski, G. A. Petersson and J. A. Montgomery Jr, *J. Chem. Phys.*, 1996, **104**, 2598–2619.
54 M. J. Frisch, G. W. Trucks, H. B. Schlegel, G. E. Scuseria, M. A. Robb, J. R. Cheeseman, G. Scalmani, V. Barone, B. Mennucci and G. A. Petersson, *et al.*, *Gaussian 16 Revision A.03*, Gaussian, Inc., Wallingford CT, 2016.
55 B. Solouki, H. Bock and R. Appel, *Chem. Ber.*, 1975, **108**, 897–913.
56 H. Ismail, P. R. Abel, W. H. Green, A. Fahr, L. E. Jusinski, A. M. Knepp, J. Zádor, G. Meloni, T. M. Selby and D. L. Osborn, *J. Phys. Chem. A*, 2009, **113**, 1278–1286.
57 B. r. K. Cunha de Miranda, C. Alcaraz, M. Elhanine, B. Noller, P. Hemberger, I. Fischer, G. A. Garcia, H. l. s. Soldi-Lose, B. Gans and L. A. Vieira Mendes, *J. Phys. Chem. A*, 2010, **114**, 4818–4830.
58 K. Voronova, K. M. Ervin, K. G. Torma, P. Hemberger, A. Bodi, T. Gerber, D. L. Osborn and B. Sztáray, *J. Phys. Chem. Lett.*, 2018, **9**, 534–539.
59 F. Gianturco and F. Schneider, *J. Chem. Phys.*, 1991, **95**, 7965–7968.
60 J. F. Todd, *Pure Appl. Chem.*, 1991, **63**, 1541–1566.
61 Vertical ionization energy, https://en.wikipedia.org/wiki/Ionization_energy#Vertical_ionization_energy.
62 R. Tuckett, J. Harvey, P. Hemberger and A. Bodi, *J. Mol. Spectrosc.*, 2015, **315**, 172–183.